A MULTIZONE, TIME–DOMAIN FINITE–VOLUME PROCEDURE FOR ELECTROMAGNETICS COMPUTATION

Vijaya Shankar, William Hall, and Alireza H. Mohammadian
Rockwell International Science Center, Thousand Oaks, CA 91360

Abstract

The differential form of the time–domain Maxwell's equations are first cast in a conservation form and then solved using a finite–volume discretization procedure derived from proven Computational Fluid Dynamics (CFD) methods applied to linear/nonlinear gasdynamics equations[1]. The formulation accounts for any variations in the material properties (time, space, and frequency dependent), and can handle thin resistive sheets and lossy coatings by positioning them at finite–volume cell boundaries. The time–domain approach handles both continuous wave (single frequency) and pulse (broadband frequency) incident excitation. Arbitrary shaped objects are modeled by using a body–fitted coordinate transformation. For treatment of complex internal/external structures with many material layers, a multizone framework with ability to handle any type of zonal boundary conditions (perfectly conducting, flux through, zero flux, periodic, nonreflecting outer boundary, resistive card, and lossy coatings, etc.) is implemented. The finite–volume procedure employs an explicit Lax–Wendroff upwind scheme to integrate Maxwell's equations in time. The time domain results are converted to the frequency domain using FFTs, and then a Green's function based near field–to–far field transformation is employed to obtain the bistatic radar cross section.

Maxwell's Equations

In order to apply CFD–based conservation–law form finite–volume methods, Maxwell's equations are rewritten in the form

$$Q_t + E_x + F_y + G_z = S \tag{1}$$

where

$$Q = \begin{Bmatrix} B_x \\ B_y \\ B_z \\ D_x \\ D_y \\ D_z \end{Bmatrix} ; E = \begin{Bmatrix} 0 \\ -D_z/\epsilon \\ D_y/\epsilon \\ 0 \\ B_z/\mu \\ -B_y/\mu \end{Bmatrix} ; F = \begin{Bmatrix} D_z/\epsilon \\ 0 \\ -D_x/\epsilon \\ -B_z/\mu \\ 0 \\ B_x/\mu \end{Bmatrix} ; G = \begin{Bmatrix} -D_y/\epsilon \\ D_x/\epsilon \\ 0 \\ B_y/\mu \\ -B_x/\mu \\ 0 \end{Bmatrix} ; S = \begin{Bmatrix} 0 \\ 0 \\ 0 \\ -J_x \\ -J_y \\ -J_z \end{Bmatrix} . \tag{2}$$

The permittivity coefficient ϵ and the permeability coefficient μ are taken to be isotropic, scalar material properties and satisfy the following relationship, $D = \epsilon\mathcal{E}$, $B = \mu\mathcal{H}$. The current density J is usually represented by $\sigma\mathcal{E}$, where σ is the material electrical conductivity.

For treatment of complex geometries, a body–fitted coordinate transformation is introduced to aid in the application of boundary conditions. Under the transformation of coordinates implied by $\tau = t$, $\xi = \xi(t,x,y,z)$, $\eta = \eta(t,x,y,z)$, $\zeta = \zeta(t,x,y,z)$, Eq. (1) can be rewritten as

$$\overline{Q}_\tau + \overline{E}_\xi + \overline{F}_\eta + \overline{G}_\zeta = \overline{S} \tag{3}$$

where

$$\overline{Q} = \begin{pmatrix} \frac{\vec{\mathcal{D}}}{J} \\ \frac{\vec{\mathcal{B}}}{J} \end{pmatrix}, \overline{E} = \begin{pmatrix} \frac{-\vec{\xi}\times\vec{\mathcal{H}}}{J} \\ \frac{\vec{\xi}\times\vec{\mathcal{E}}}{J} \end{pmatrix}, \overline{F} = \begin{pmatrix} \frac{-\vec{\eta}\times\vec{\mathcal{H}}}{J} \\ \frac{\vec{\eta}\times\vec{\mathcal{E}}}{J} \end{pmatrix}, \overline{G} = \begin{pmatrix} \frac{-\vec{\zeta}\times\vec{\mathcal{H}}}{J} \\ \frac{\vec{\zeta}\times\vec{\mathcal{E}}}{J} \end{pmatrix}, \text{ and } \overline{S} = \begin{pmatrix} \frac{-\vec{\mathcal{J}}}{J} \\ 0 \end{pmatrix}. \tag{4}$$

where $J = |\partial(\xi,\eta,\zeta)/\partial(x,y,z)|$ is the Jacobian of the transformation and, *e.g.*, $\vec{\xi} = (\partial_x\xi, \partial_y\xi, \partial_z\xi)$. The two–dimensional transverse magnetic (TM) and transverse electric (TE) equations are special cases of Eq. (4).

Finite–Volume Treatment

Associating the subscripts j,k,ℓ with the ξ,η,ζ directions, a numerical approximation to Eq. (3) may be expressed in the semi–discrete conservation law form given by

$$\left(\widehat{Q}_{j,k,\ell}\right)_\tau + \left(\widehat{E}_{j+1/2} - \widehat{E}_{j-1/2}\right) + \left(\widehat{F}_{k+1/2} - \widehat{F}_{k-1/2}\right) + \left(\widehat{G}_{\ell+1/2} - \widehat{G}_{\ell-1/2}\right) = \widehat{S}_{j,k,\ell} \tag{5}$$

where $\widehat{E}, \widehat{F}, \widehat{G}$ are numerical or representative fluxes at the bounding sides of the cell for which discrete conservation is considered, and $\widehat{Q}_{j,k,\ell}$ is the representative conserved quantity (the numerical approximation to $\overline{Q}$) considered conveniently to be the centroidal value. The half–integer subscripts denote cell sides and the integer subscripts the cell itself or its centroid.

Flux Evaluation

In order to evaluate the fluxes $\widehat{E}$, $\widehat{F}$, and $\widehat{G}$, characteristic theory is employed[2] at cell interfaces. Referring to Fig. 1, given a left state $(-)$ and a right state $(+)$ on either side of an interface, the interface fluxes can be obtained from

$$\begin{aligned}
\widehat{\xi}\times E^* &= \widehat{\xi}\times \frac{\left\{\left[E^+(\epsilon c)^+ + \widehat{\xi}\times H^+\right] + \left[(\epsilon c)^- E^- - \widehat{\xi}\times H^-\right]\right\}}{(\epsilon c)^- + (\epsilon c)^+ + \sigma d} \\
\widehat{\xi}\times H^* &= \widehat{\xi}\times \frac{\left\{\left[1+\sigma d(\mu c)^+\right]\left(H^-(\mu c)^- + \widehat{\xi}\times E^-\right) + \left[(\mu c)^+ H^+ - \widehat{\xi}\times E^+\right]\right\}}{(\mu c)^+ + (\mu c)^- + \sigma d(\mu c)^+(\mu c)^-} \\
\widehat{\xi}\times H^{**} &= \widehat{\xi}\times \frac{\left\{\left[1+\sigma d(\mu c)^-\right]\left((\mu c)^+ H^+ - \widehat{\xi}\times E^+\right) + \left[(\mu c)^- H^- + \widehat{\xi}\times E^-\right]\right\}}{(\mu c)^+ + (\mu c)^- + \sigma d(\mu c)^-(\mu c)^+}
\end{aligned} \tag{6}$$

The resistive sheet is modeled by σd where σ is the conductivity and d is the thickness. When $\sigma d = 0$, the total tangential electric and magnetic fields are continuous across a

material interface. When $\sigma d \rightarrow \infty$, the resistive sheet represents a perfectly conducting surface, and the total tangential electric field $\widehat{\xi} \times E^*$ goes to zero satisfying Maxwell's boundary conditions for a perfectly conducting surface. Equation (6) allows for the material properties (ϵ, μ) to jump any amount at an interface.

Multizone Arrangement

For treatment of complex internal/external structures with many material layers, a multizone framework with ability to handle any type of zonal boundary conditions is implemented. Figure 2 illustrates a structured airfoil case where multizoning is very attractive for modeling the scatterer and the field around it. Zone to zone communication is provided through prescription of appropriate zonal boundary conditions. Once the zoning arrangement is made, the following steps are carried out: 1) grid each zone separately using a body–fitted grid generator such that all zonal boundaries are constant coordinate surfaces, allowing for easy implementation of boundary conditions; 2) specify material properties for each finite–volume cell in each zone; 3) specify the type of zonal boundary conditions; and 4) for each zone side, specify the neighboring zone number and the neighboring zone side.

Code Structure

The code is constructed in a modular form where the Maxwell solver can accommodate any geometry/materials package. The vectorized code runs on a single processor CRAY/X–MP at 80 MFLOPS rate, requiring 1.8×10^{-6} seconds/time step/grid point. The code is also being modified to run on a CRAY/Y–MP with micro/macro tasking options and is expected to produce speedup of more than 1 GFLOPS.

Results

To illustrate the capability of the multizone EM code, two–dimensional results are shown in Fig. 3 for a dielectric shell problem using a three–zone gridding. A typical TM or a TE case using a total of 2500 grid points takes 4 seconds on a CRAY/X–MP to provide the bistatic RCS for a continuous wave (single frequency) case. Figure 4 shows results for a layered airfoil case using a ten–zone gridding.

A three–dimensional version of the code employing multiprocessor options is presently in the debugging stage. The objective is to achieve more than a GFLOPS rate on CRAY/Y–MP, CRAY–2 architectures.

References

1. Shankar, V. and Chakravarthy, S.R., "Development and Application of Unified Algorithms for Problems in Computational Science," invited paper presented at the NASA Conference on Supercomputing in Aerospace, NASA Ames Research Center, March 10–12, 1987.

2. Lax, P., "Hyperbolic Systems of Conservation Laws and the Mathematical Theory of Shock Waves," SIAM, Philadelphia, 1973.

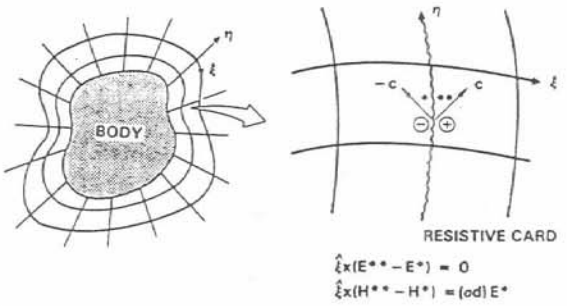

Fig. 1. Interface flux treatment with a resistive sheet.

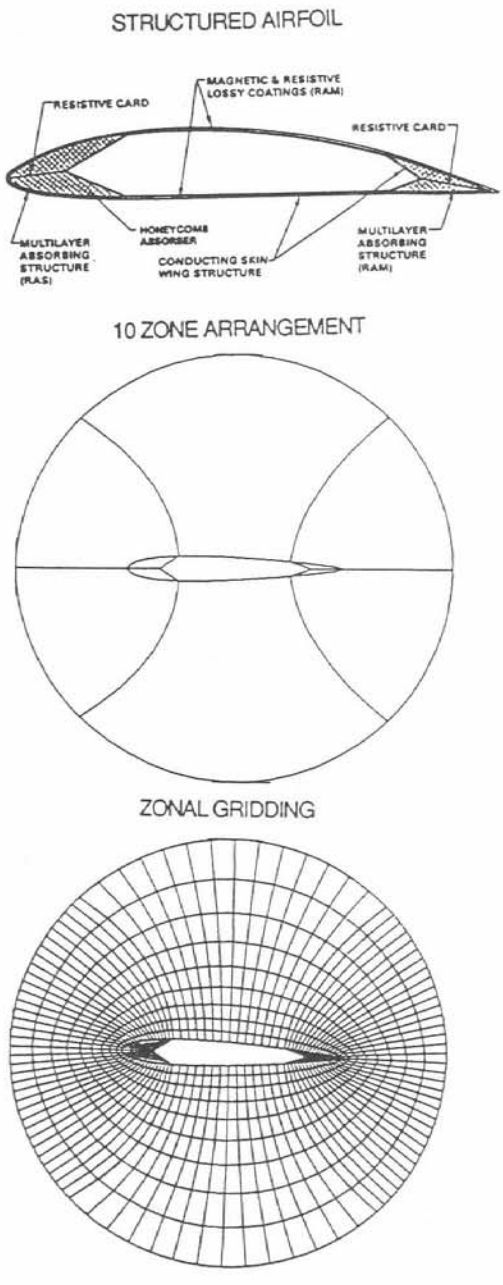

Fig. 2. Multizone arrangement.

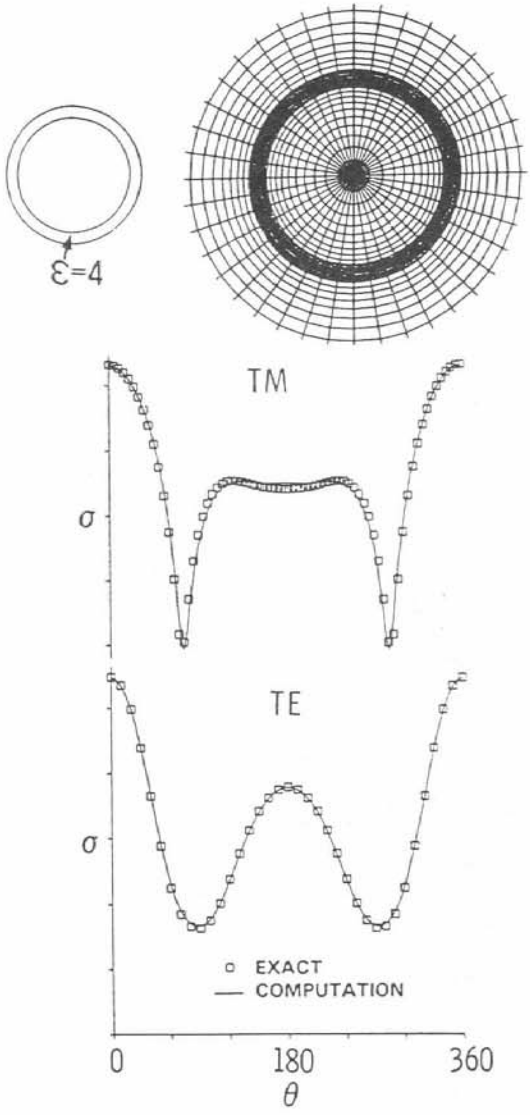

Fig. 3. TM and TE RCS results for a dielectric shell.

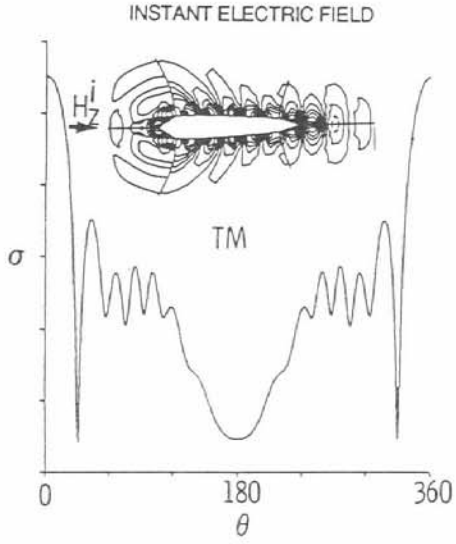

Fig. 4. RCS for a structured airfoil.